RESEARCH ARTICLE

NANO · MICRO small
www.small-journal.com

Calix[4]pyrrole-Based Wavy Covalent Organic Framework: A Protective Layer for High Performance Lithium-Metal Batteries

Jinya Tian, Yaqi Liao, Yaling Zhu, Yi Li, Yanlei He, Jianqiao Zhou, Yonggang Yao, Lixia Yuan, Jonathan L. Sessler,* Yunhui Huang,* and Xiaodong Chi**

Practical applications of lithium metal batteries are often limited by low cycling efficiencies and uncontrolled lithium dendrite growth caused by unstable and heterogeneous lithium-electrolyte interfaces. To address this issue, a calix[4]pyrrole-based wavy covalent organic framework (WCOF) is developed that acts as a protective layer to suppress Li dendrite growth and reduce side reactions on the Li anode. The present WCOF is porous and contains calix[4]pyrrole units acting as "molecular traps" that allow efficient PF_6^- anion capture while allowing for uniform Li^+ diffusion. This provides structurally stable artificial protective layers that permit high Li^+ transference numbers. The resulting solid electrolyte interphases permit ultralong-term stable cycling at a current density of 1 mA cm^{-2} and reversible lithium plating/stripping (over 2500 h) at an areal capacity of 2 mAh cm^{-2}. The protected anodes of this study also demonstrated excellent cell stability through 260 cycles when paired with high-voltage cathodes (NCM811 with high mass loading: 20 mg cm^{-2}).

1. Introduction

Batteries with Li metal anodes (LMAs) show considerable potential as next-generation energy storage devices due to their high theoretical specific capacity (3860 mAh g^{-1}).[1] However, LMAs suffer from several intrinsic limitations, which have precluded their use in various practical applications. One critical issue is the high chemical reactivity of LMAs. They react readily with organic electrolytes, resulting in the formation of a non-uniform solid electrolyte interphase (SEI) layer on the surface of the lithium metal.[2] The non-uniformity of the SEI lead to irregular Li^+ diffusion and continuous cracking of the initially formed SEI, which exposes fresh Li surfaces to the electrolyte.[3] Ultimately, this leads to reduced coulombic efficiency and accelerated battery failure, particularly under the high current densities and the large areal capacities required for next-generation batteries.[4] There is thus a need for alternative artificial coatings to supplant the native solid electrolyte interface (SEI), attaining stable lithium metal anodes.[5] Ideally, these coatings should be endowed with ordered lithium ion transport channels and anion regulation capabilities. Here, we report a calix[4]pyrrole-based wavy covalent organic framework (**WCOF**) that acts as a protective layer to suppress Li dendrite growth and mitigate side reactions at the Li anode. The present **WCOF** contains calix[4]pyrrole anion "traps" within porous inner cores. It thus permits the formation of a structurally stable artificial protective layer with efficient PF_6^- anion capture and uniform Li^+ diffusion while providing high Li^+ transference numbers. As detailed below, the use of these artificial coatings allowed for ultralong-term stable cycling at a current density of 1 mA cm^{-2}, as well as reversible lithium plating/stripping (over 2500 h) at an areal capacity of 2 mAh cm^{-2}.

Covalent organic frameworks (COFs) have emerged as an important class of porous materials due to their well-defined structures, tunable pore functionality, and excellent chemical stability.[6] They have demonstrated utility in a variety of applications, including catalysis,[7] adsorption,[8] drug delivery,[9] and ion conduction.[10] Typically composed of polyaromatic building blocks, COFs can be produced as either 2- or 3D structures.[10a,11] However, attempts to incorporate macrocyclic components into COFs have been limited to shape-persistent macrocycles with inherent rigidity, such as cyclodextrins and arylene-ethylene macrocycles.[10a,12] The use of conformationally flexible molecules, such as calix[4]pyrroles, to construct COFs remains challenging. Addressing this challenge might allow the

J. Tian, Y. Liao, Y. Zhu, Y. Li, Y. He, J. Zhou, Y. Yao, L. Yuan, Y. Huang, X. Chi
State Key Laboratory of Materials Processing and Die & Mold Technology
School of Materials Science and Engineering
Huazhong University of Science and Technology
Wuhan 430074, China
E-mail: yuanlixia@hust.edu.cn; huangyh@hust.edu.cn; xchi@hust.edu.cn

J. L. Sessler
Department of Chemistry
The University of Texas at Austin
Austin, TX 78712-1224, USA
E-mail: sessler@cm.utexas.edu

X. Chi
Shenzhen Huazhong University of Science and Technology Research Institute
Shenzhen 518000, China

The ORCID identification number(s) for the author(s) of this article can be found under https://doi.org/10.1002/smll.202506365

DOI: 10.1002/smll.202506365

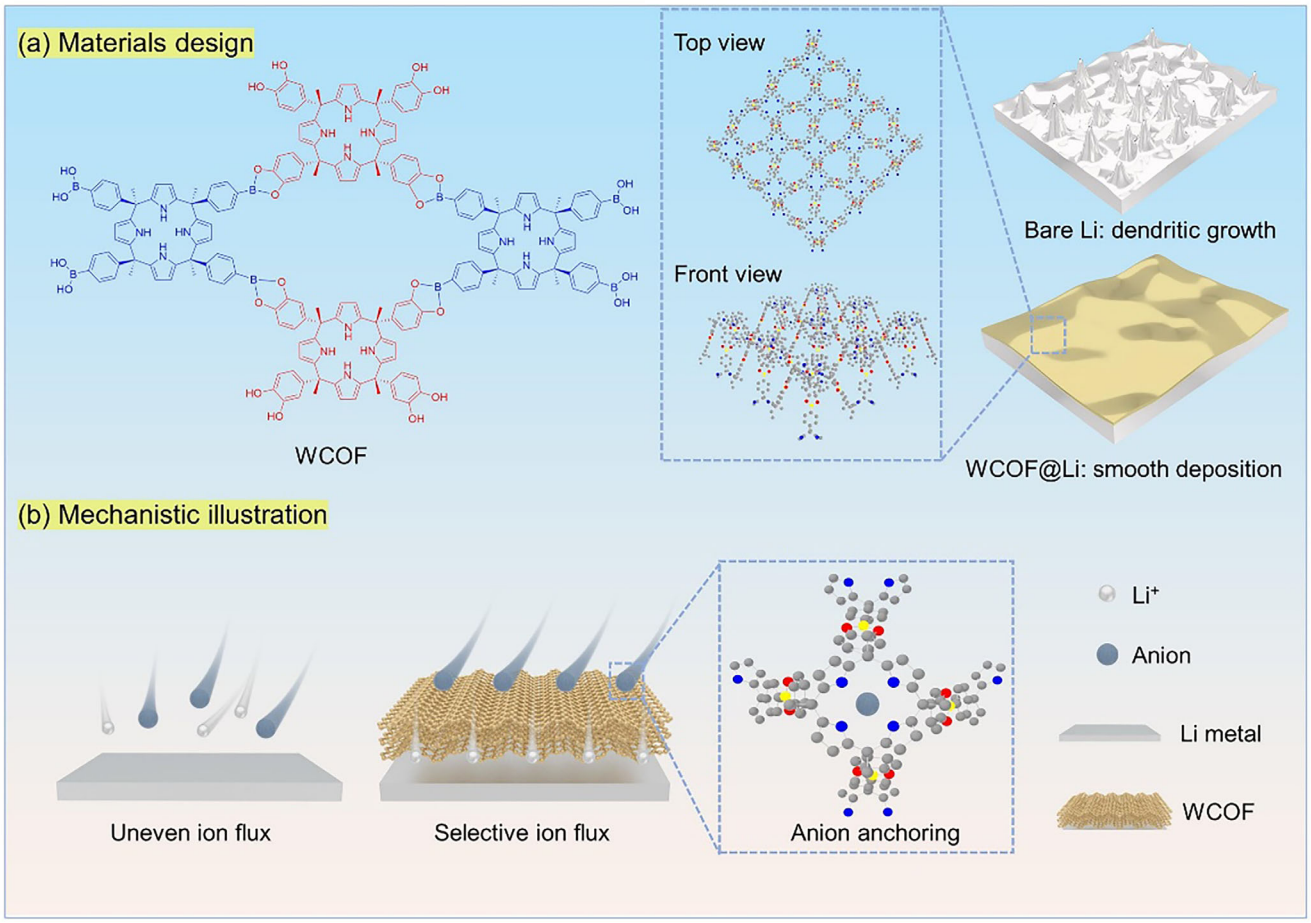

Scheme 1. Illustration of the molecular-level design of an artificial coating using a calix[4]pyrrole (**C4P**)-based wavy covalent organic framework. a) Chemical structure and artificial coatings derived from the **WCOF** of this study. The **WCOF** forms a dense layer (yellow) that blocks electrolyte access to the surface. b) Mechanistic illustration showing the selective ion flux expected to induce uniform Li^+ diffusion and produce a high Li^+ transference number.

construction of COFs that are tailored to specific applications, such as synthetic coatings-based protection of lithium anodes.

Calix[4]pyrroles are macrocycles composed of four pyrrole units connected by fully substituted meso-carbon atoms, which enable them to recognize various anionic and neutral electron-rich species through stabilizing pyrrolic —NH hydrogen bonding interactions.[13] Strongly bound guests can promote the conversion of the stable 1,3-alternate conformation to the corresponding cone form. The unique properties of calix[4]pyrroles make them a versatile building block for creating a wide range of supramolecular structures, including self-assembled capsules,[14] stimulus-responsive polymers,[15] ion-pair receptors,[16] anion transport agents,[17] extractants, molecular frameworks,[18] and sensors.[19] Calix[4]pyrroles have also proved amenable to structural modification. Inspired by their synthetic accessibility, anion binding characteristics, and conformational flexibility, we considered it likely that calix[4]pyrroles could be used to create functionalized COFs that would act as artificial LMA-stabilizing coatings that improve the performance of Li metal batteries (**Scheme 1**). The present study was undertaken to test this possibility.

2. Results and Discussion

2.1. Synthesis and Structural Analysis of C4Ps and WCOF

The specific choice of calix[4]pyrrole (**C4P**) (**Figure 1**a,c) as the core anion recognition element was dictated by the fact that it could be readily functionalized with phenylboronic acid and catechol functionalities that would support COF construction through self-assembly of the peripheral —OH and $-B(OH)_2$ groups. The key monomers in question, **C4P-1** and **C4P-2**, were prepared *via* one-pot syntheses. The preparation and characterization of the monomers are detailed in Figures S1–S8 (Supporting Information). Single crystals suitable for X-ray diffraction analysis were grown by slow evaporation of DMF (**C4P-1**) and acetone (**C4P-2**), respectively. The resulting structures revealed that both **C4Ps** adopt bowl-like conformations (Figure 1b,d) and that each **C4P-2** macrocycle interacts with two nearest neighbors through phenylboronic acid O–H•••O hydrogen bonds to form a wavy hydrogen-bonded organic framework (Figure S9, Supporting Information). Both calix[4]pyrroles possess relatively deep cavities rich in NH donor sites, which were expected to

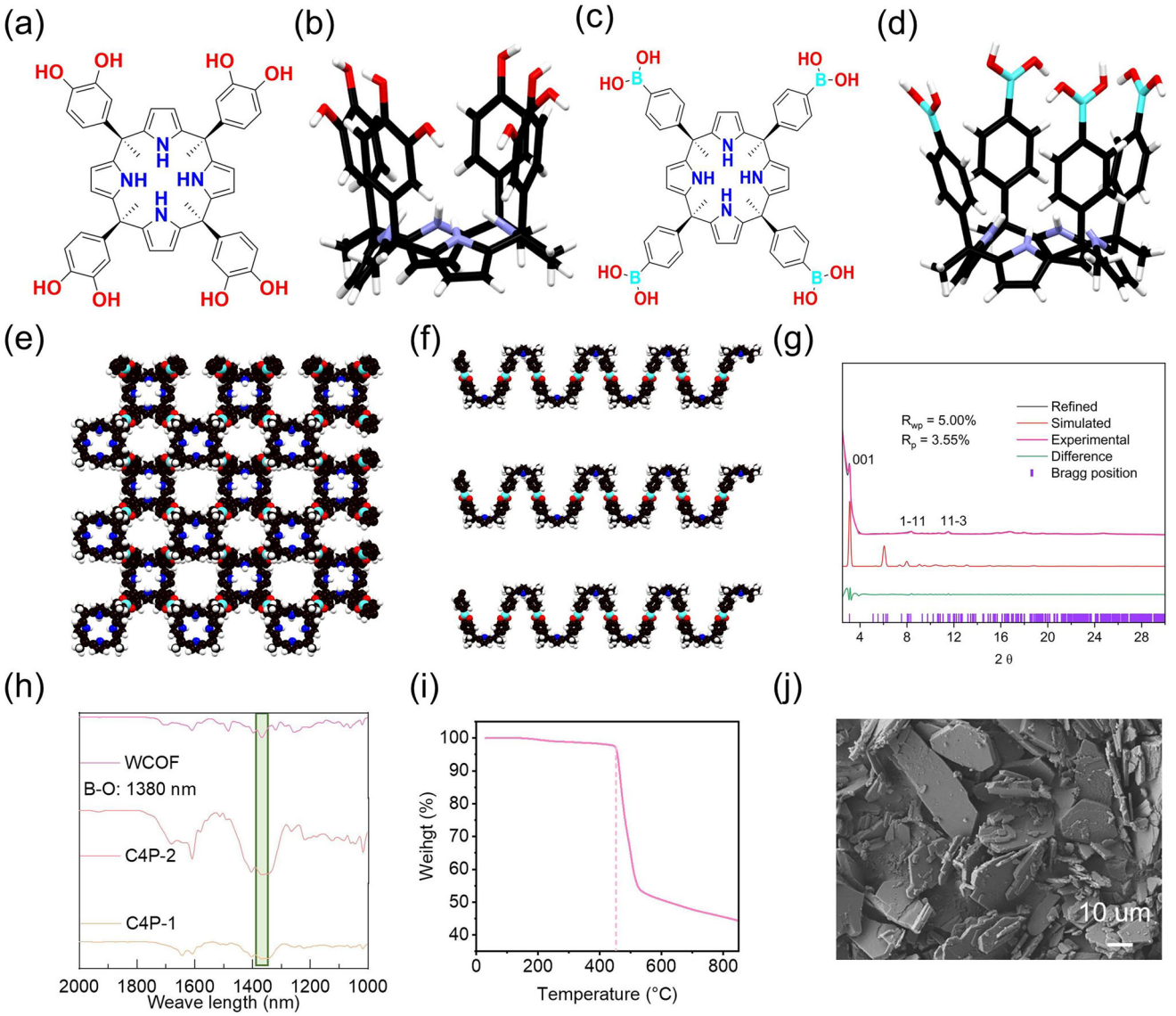

Figure 1. Chemical and corresponding single crystal structures of **C4Ps** and the **WCOF** structure analysis. a) Chemical structures of **C4P-1**. b) Single crystal structures of **C4P-1**. c) Chemical structures of **C4P-2**. d) Single crystal structures of **C4P-2**. e) Top view of the **WCOF**, showing the layer stacking and heteropores within the structures. f) Side view showing the layer stacking of **WCOF** and its wavy nature. g) PXRD profiles of the **WCOF**. Experimentally observed (black), Pawley refined (red dash) and their difference (green), simulated (pale blue) using the AA stacking mode. h) FT-IR spectrum of **C4P-1**, **C4P-2**, and **WCOF**. i) Thermogravimetric analysis of **WCOF**. j) SEM image of **WCOF** at a scale bar of 10 um.

enhance their anion recognition features that are a hallmark of **C4P** chemistry (Figure 1b,d). Indeed, considerable prior work has served to confirm that **C4P** is capable of anion binding.[14,19] For the present study, we performed theoretical calculations on the electrostatic potential of one of the **C4Ps** containing an −OH group (**C4P-1**). These calculations revealed that the —NH functional group within the cavity carries a partial positive charge of ≈0.11 eV (Figure S10, Supporting Information). This was expected to abet anion recognition. ^{1}H NMR spectroscopic studies provided further support for this design expectation. As shown in Figure S11 (Supporting Information), upon the addition of 1 equiv. of $LiPF_6$ to a solution of **C4P-1** in dimethyl sulfoxide-d_6 (DMSO-d_6), downfield chemical shift changes characteristic of pyrrole NH—anion interactions were observed. These findings support the conclusion that **C4P** would act as an effective PF_6^- anion trap. Moreover, due to the flexibility of the calix[4]pyrrole units,[20] **WCOF** was expected to retain the adaptability and anion recognition capability of its constituent **C4P** monomers. We thus sought to explore whether COFs based on **C4P** would prove useful as coatings in lithium-metal battery applications.

To test the above possibility, a wavy covalent organic framework (**WCOF**) was synthesized by heating suspensions of **C4P-1** and **C4P-2** in acetone for 3 days (see Figures S12–S16, Supporting Information). The crystallinity of the **WCOF** was confirmed by powder X-ray diffraction (PXRD) and transmission electron microscopy (TEM) analyses. Structural characterization was

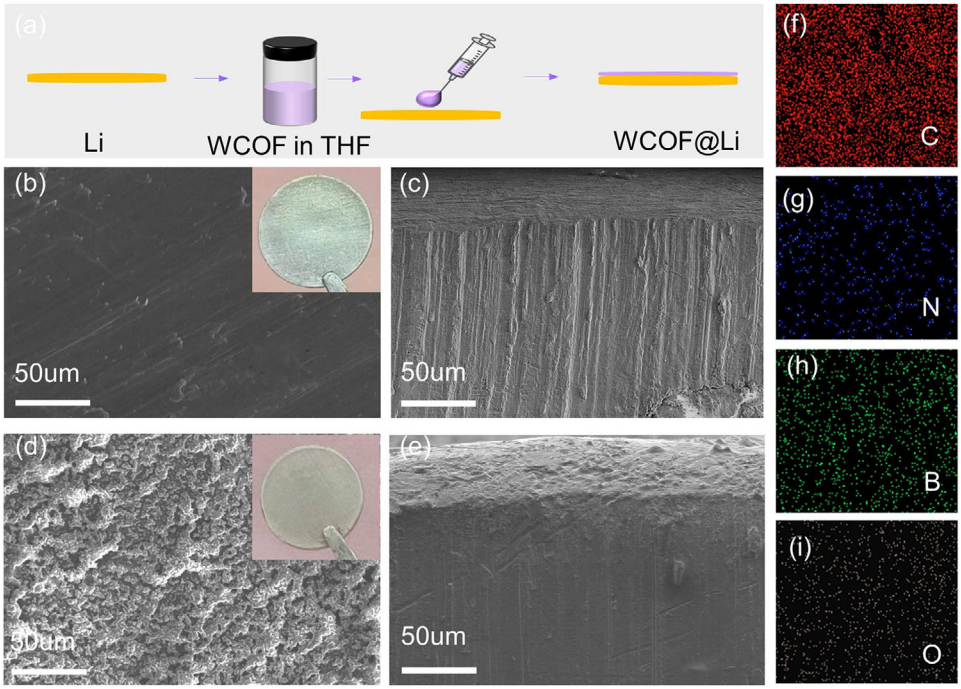

Figure 2. Characterization of synthetic protective layers. a) Schematic illustration of the process of drop-casting the **WCOF** of this study onto a Li metal anode. b) SEM view of the surface of bare Li. The inset digital image shows a bare Li metal anode. c) SEM cross-section view of the bare Li metal anode. d) SEM view of the surface of **WCOF**@Li metal anode. The inset digital image shows the **WCOF**@Li metal anode. e) SEM cross-section view of **WCOF**@Li metal anode. f–i) Elemental mapping images of the surface SEM images of **WCOF**@Li: f) C g) N, h) B, and i) O.

performed using computational modeling (Figure 1e,f) in combination with PXRD studies (Figure 1g). The best agreement between the experimental and simulated PXRD patterns was obtained for a triclinic structure in the *P1* space group, with unit cell parameters of a = 16.83 Å, b = 16.43 Å, and c = 28.61 Å. A Pawley refinement based on this unit cell yielded an excellent fit to the experimental data, supporting the validity of the proposed structural model. Notably, the model reveals that the two **C4P** units are connected at opposite ends (Figure 1f), resulting in a wavy topology. This is a distinct geometric feature that sets **WCOF** apart from most periodic COFs reported to date. The diffraction peak at $2\theta = 3.71°$ is the most intense and matches well with the refined pattern, validating the quality of the crystallographic fit. High-resolution transmission electron microscopy (HRTEM) further supports the crystalline nature of **WCOF**. As shown in Figure S17a (Supporting Information), Well-defined lattice fringes with a periodicity of ≈1.1 nm were observed (cf. Figure S17a, Supporting Information). This is as would be expected for a system with high crystallinity. The diffraction data (cf. Figure S17d, Supporting Information) also support the conclusion that **WCOF** has a crystalline structure. Moreover, the selected area electron diffraction (SAED) pattern (Figure S17d, Supporting Information) exhibits clear diffraction spots, further supporting the ordered crystalline nature of the material. Such findings support the conclusion that the frameworks possess long-range order. An N_2 adsorption isotherm for **WCOF** revealed a BET surface area value of 8.46 $m^2\ g^{-1}$ (Figure S18, Supporting Information). Thermogravimetric analyses (TGA) of the resulting light purple powder provided evidence that the **WCOF** is stable up to 445 °C (Figure 1i). Scanning electron microscopy (SEM) studies revealed an aggregation morphology of thin flakes for the **WCOF** (Figure 1j), in agreement with its layered and wavy nature. The solid-state ^{13}C CP-MAS NMR (Figure S15, Supporting Information) is characterized by the presence of signals for the sp^2 hybridized aromatic carbons (δ = 120–160 ppm), the pyrrole rings (δ = 90–110 ppm), and the *meso*-methyl/methylene groups (δ = ≈36.5 and ≈20 ppm). This is taken as evidence for the structural integrity of the calix[4]pyrrole units being retained in the **WCOF**. Fourier transform infrared (FTIR) spectra (Figure 1h) exhibit a sharp B—O stretching peak at 1380 cm^{-1}, indicating successful formation of borate ester linkages and completion of the condensation reaction to the limits of detection.[6]

2.2. Synthetic Protective Layers Preparation and Their Electrochemical Stability

To create a putative protective layer for LMAs, a suspension of the light purple **WCOF** was cast onto a Li surface (**Figure 2a**; Figures S20 and S21, Supporting Information). As shown in the resulting scanning electron microscopy (SEM) images and corresponding elemental mapping (Figure 2b–i; Figure S22, Supporting Information), the **WCOF** adheres tightly and uniformly to the Li metal surface. The results from infrared experiments provide additional support for the conclusion that **WCOF** remains stable throughout the battery cycling process. Specifically, FT-IR spectroscopy was used to monitor the B—O bonding in the **WCOF** powder. The infrared absorption peak corresponding to the B—O bond in borate at 1380 cm^{-1} remains present and unchanged

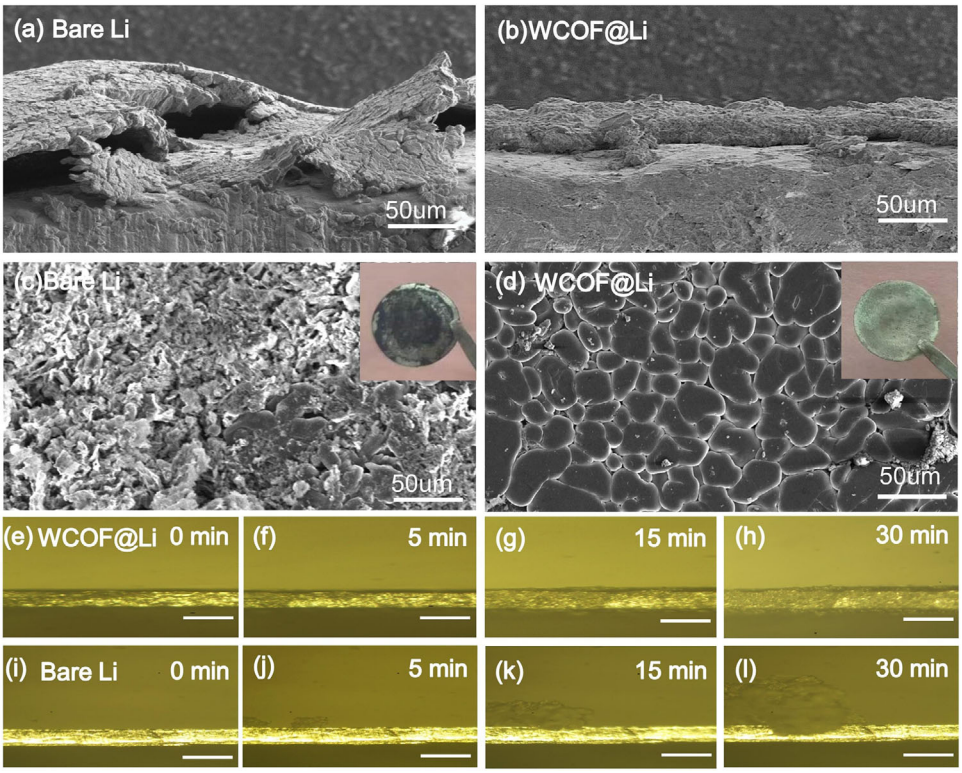

Figure 3. Electrode morphologies and in situ observation of Li deposition. a) SEM cross-section images of Li metal deposition on bare Li. b) SEM cross-section images of Li metal deposition on **WCOF**@Li plate. c) SEM images of Li metal deposition on bare Li plate (50 cycles, 1 mA cm^{-2}, 4 mAh cm^{-2}) in symmetrical cells were tested. d) SEM images of Li metal deposition on **WCOF**@Li plate (50 cycles, 1 mA cm^{-2}, 4 mAh cm^{-2}) in symmetrical cells were tested. e–h) In situ optical microscopy images of Li deposits on **WCOF**@Li anodes upon discharging for 0, 5, 15, and 30 min at a current density of 2 mA cm^{-2}. Scale bars: 25 µm. i–l) In situ optical micros-copy images of Li deposits on bare Li anodes upon discharging for 0, 5, 15, and 30 min at a current density of 2 mA cm^{-2}. Scale bars: 25 µm.

after 50 cycles at 1 mA cm^{-2} and 4 mAh cm^{-2} (Figure S23, Supporting Information). In situ Raman spectroscopy further corroborates this finding (Figure S24, Supporting Information). Distinct vibrational peaks corresponding to B—O bonds in boronic acid esters at 1340 cm^{-1} and C═C bonds in benzene rings at 1580 cm^{-1} were clearly observed, confirming the structural integrity of the **WCOF** protective layer during operation. The stability of **WCOF** was also confirmed by the detection of B—O and B-C bonds in the XPS analysis of the lithium metal surface and **WCOF** powder after 50 cycles at 1 mA cm^{-2} 4 mAh cm^{-2} test conditions (Figure S25, Supporting Information). Notably, the XPS peak positions of **WCOF** on the lithium metal surface shift compared to those of pure **WCOF**, indicating interactions with other chemical species.

The electrochemical stability of **WCOF**@Li was further explored at the electrode-electrolyte interface. We conducted a detailed examination of lithium metal deposition behavior on both bare lithium and **WCOF**@Li electrodes using SEM. Highly porous Li dendrites were observed on the bare Li electrode after Li deposition at 1 mA cm^{-2} for 50 cycles (**Figure** 3a,c). In contrast, under the same experimental conditions, a pebble-like compact deposition without dendritic Li deposits is seen for the Li electrode bearing a **WCOF** protective layer (Figure 3b,d). Presumably, this reflects a reduction in the ion concentration gradient and promotion of rapid and homogeneous interfacial ion migration, leading to a more uniform Li surface (Figure 3d).

The *in situ* morphological evolution of the Li metal anodes after cycling of symmetric Li|Li cells was also monitored (Figure 3e–l). As shown in Figure 3e,l, and Figure S26 (Supporting Information), both the **WCOF**@Li and bare Li anodes presented a smooth surface before Li plating. A dendrite-free flat surface was seen for the **WCOF**@Li anode that was maintained throughout the plating process (Figure 3e–h). However, the bare Li anode started to generate mossy Li by 5 min with the formation of numerous dendrites being formed during the ensuing 30 min (Figure 3i–l). These findings were taken as further evidence of the putative advantages of the **WCOF** protective layer for stabilizing electrode-electrolyte interfaces and suppressing uncontrolled dendritic Li deposition in lithium metal batteries.

2.3. Electrochemical Performance and Mechanism of Li^+ Transport Studies

The Li^+ transference number (t_{Li^+}) was then measured to evaluate quantitatively the Li^+ conducting ability of the **WCOF** protective layer. The unadorned (bare) symmetric Li cell exhibited a relatively low t_{Li^+} of 0.39, presumably reflecting the relatively high migration speed of the counteranions compared to the solvated Li^+

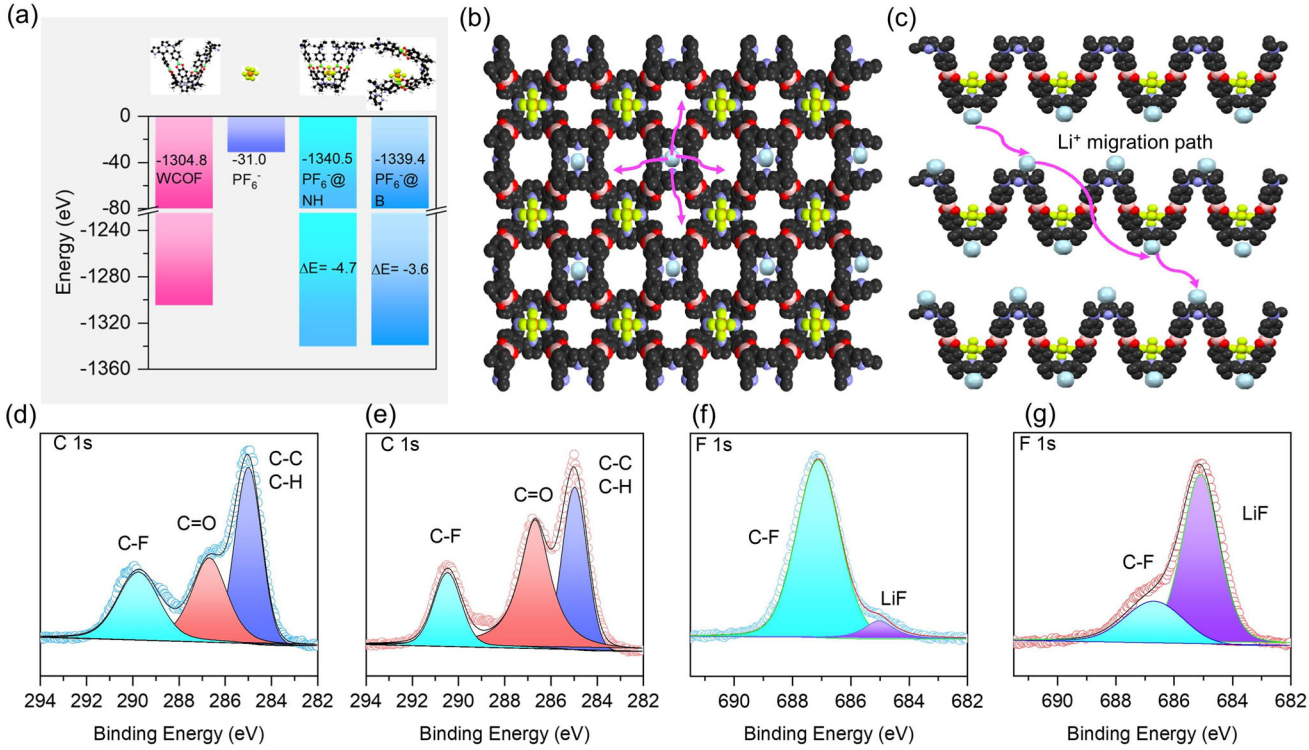

Figure 4. Proposed mechanism of Li^+ transport showing the anion trapping expected within the **WCOF** layer. a) DFT calculations involving different anion binding models and the corresponding calculated anion binding energies; b) top view and c) side view showing the proposed transport of Li^+ through the pore of the **WCOF** layer, with the counterions being confined within the calix[4]pyrrole cavity. d–g) XPS spectra of the cycled bare Li surface for d) C 1s and f) F 1s. XPS spectra of the cycled **WCOF**@Li surface for e) C 1s and g) F 1s.

cations. The corresponding value was 0.79 for **WCOF**@Li (Figure S27, Supporting Information). This increase is ascribed to anion trapping by the **C4P** subunits within the protective **WCOF** layer and hence a suppression of the Li^+ concentration gradient at the interface. Density functional theory (DFT) calculations were conducted to obtain insights into the mechanism of Li^+ transport through the **WCOF** layer (**Figure 4a** a; Figure S28, Supporting Information). As shown in Figure 4b, while the anions tend to remain inside the cavity of calix[4]pyrrole, being held there through hydrogen bonding and Lewis acid-base interactions, the Li^+ ions are transported through the pores of the **WCOF** layer, resulting in a relatively uniform Li^+ flux and a high Li^+ transference number (Figure 4c). Furthermore, X-ray photoelectron spectroscopy (XPS) provided additional insights (Figure 4d–g; Figure S29, Supporting Information). The XPS image of the bare Li surface after cycling is shown in Figure 4f; it reveals a reduced LiF level compared to the **WCOF**@Li surface (Figure 4g). These XPS results served to confirm the ability of **WCOF** to bind with anions, thereby validating its role in enhancing the formation of LiF and improving lithium metal anode stability.

Galvanostatic cycling tests were performed on symmetric Li|Li cells to assess the Li plating/stripping performance of **WCOF**-protected Li anodes. As shown in **Figure 5a**, the bare Li anode displayed relatively poor electrochemical cycling, with a gradual increase in voltage hysteresis and failure being observed over the course of 650 h. These performance shortcomings are attributed to the elevated charge transfer resistance caused by electrical disconnection, as well as electrolyte depletion ascribed to the repeated growth and corrosion of Li dendrites. In contrast, the **WCOF**@Li anode provided a highly stable voltage plateau, even after cycling for over 2500 h at a controlled Li plating/stripping capacity of 2 mAh cm^{-2} at 1 mA cm^{-2} (Figure 5a).

To explore further the putative benefits of the **WCOF** modification, symmetric cells were tested at 4 mAh cm^{-2}. It was found that the **WCOF**-modified symmetric cells exhibited a reduced overpotential and displayed an extended cycle life, lasting over 500 h (Figure 5b). In addition, the efficacy of the **WCOF** coatings was evaluated in ether-based electrolytes, yielding 800 h of stable cycling at 1 mA cm^{-2} and 4 mAh cm^{-2} (Figure S30, Supporting Information). In aggregate, these findings underscore the versatility of the present **WCOF** coating across a wide range of electrolyte systems and highlight its potential to improve the stability and performance of lithium metal batteries.

To test the potential utility of the **WCOF** protective layer, Li metal coin cell batteries were assembled by pairing the **WCOF**@Li anode with a high-voltage $LiNi_{0.8}Mn_{0.1}Co_{0.1}O_2$ (NCM811) cathode (active material loading: 20 mg cm^{-2}). As expected, the **WCOF**@Li anode exhibited excellent cycling stability and rate performance compared to a bare Li anode when paired with a high-voltage NCM811 cathode in a coin cell. The **WCOF**@Li|NCM811 coin cell cycled at 0.5 C exhibited a high initial capacity of 181.3 mAh g^{-1} and excellent capacity retention of 91.3% with an average coulombic efficiency (CE) of 99.8% over 260 cycles (Figure 5c; Figures S31 and S32 and Table S1,

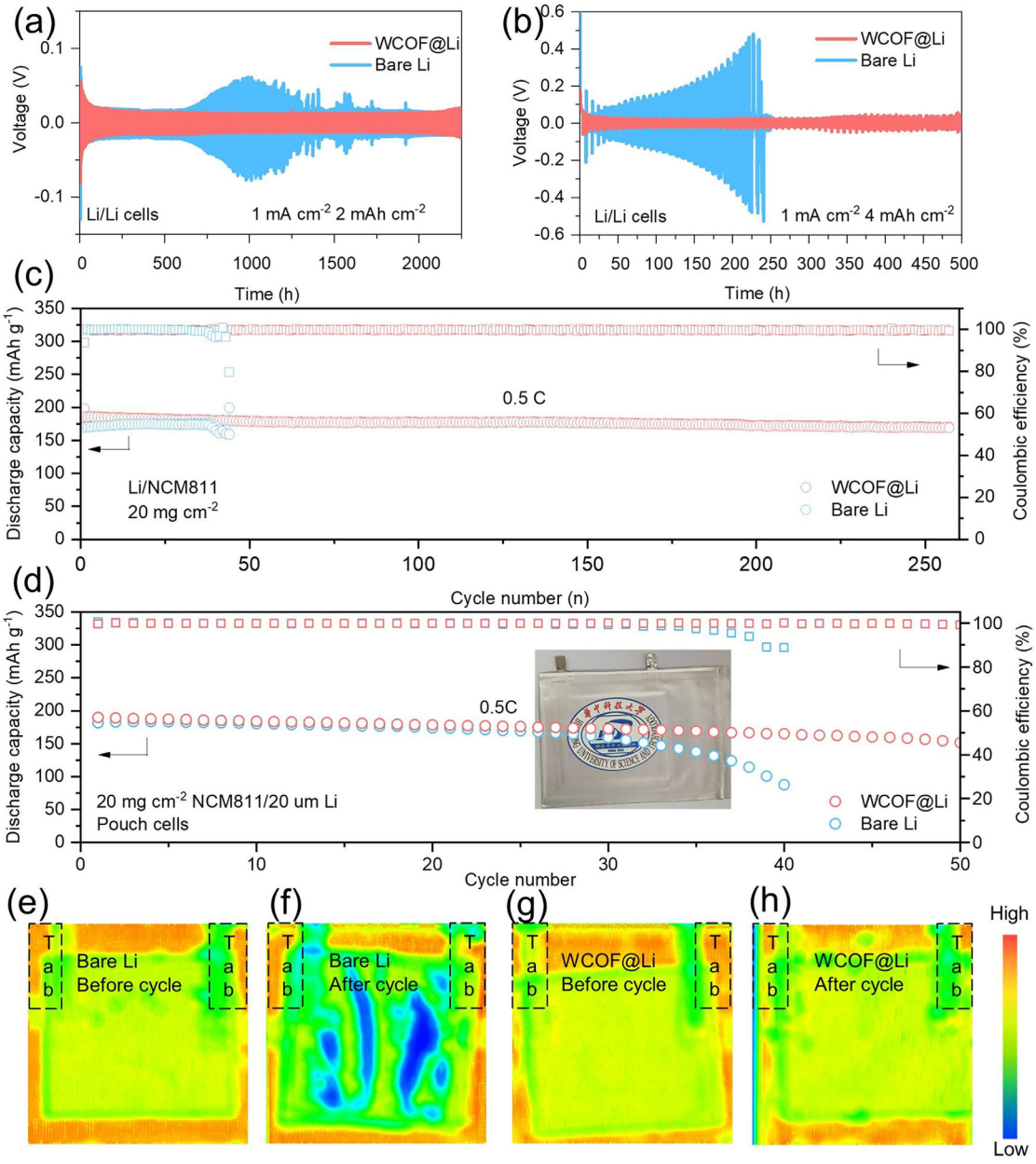

Figure 5. Electrochemical performance of symmetric Li|Li and Li|NCM811 cells. a) Cycling stability of unadorned (bare) Li/Li and **WCOF**@Li/Li cells at current densities of 1 mA cm^{-2} with areal capacities of 2 mAh cm^{-2}. b) Cycling stability of unadorned (bare) Li/Li and **WCOF**@Li/Li cells at current densities of 1 mA cm^{-2} with areal capacities of 4 mAh cm^{-2} in ester electrolytes. c) Cycling stability of Li/NCM811 and **WCOF**@Li/NCM811 coin cells with high loadings (20 mg cm^{-2}) at 0.5 C. d) Pouch cells with 20 mg cm^{-2} loadings at 0.5 C. The insert shows the pouch cell. e–h) Ultrasonic transmission mapping of the Li/NCM811 and **WCOF**@Li/NCM811 pouch cells e,g) before cycling; f,h) after 15 cycles at 0.5 C.

Supporting Information).[21] In contrast, the bare Li|NCM811 coin cell underwent rapid capacity degradation for 40 cycles. Meanwhile, the self-discharge test of the Li|NCM811 battery shows that the voltage stability of the real sample is better than that of the blank sample, as shown in Figure S33 (Supporting Information). Notably, the cell with the **WCOF**@Li anode exhibited excellent rate performance, delivering discharge capacities of 194.3, 181.1, 161.7, 141.4, 105.8, 78.7, and 60.7 mAh g^{-1} at 0.1, 0.2, 0.5, 1, 2, 3, and 5 C, respectively (Figures S34 and S35, Supporting Information). In contrast, the cell made up using a bare Li anode showed inferior rate performance. These results support the design expectation that the **WCOF** of the present study may have a role to play in inhibiting the growth of Li dendrites and ensuring the stability of electrolyte/electrode interfaces in lithium metal batteries.

To explore the scale-up potential of the **WCOF** protective layer, a **WCOF**@Li|NCM811 full battery was assembled in the form of a pouch cell (Figures S36 and S37, Supporting Information).

As shown in Figure 5d, the capacity of the pouch cell with the **WCOF**@Li anode exhibited cycle stability over 50 cycles. Conversely, the capacity of an analogous pouch cell with unadorned (bare) Li anodes displayed significant decay over the course of only 25 cycles. Ultrasonic scanning was used to monitor the gas generation inside the pouch cells.[22] This technique relies on the fact that ultrasonic signals transmitted through gas-liquid or gas-solid interfaces are subject to interfacial impedance, which leads to a reduction in signal transmission. To aid in visualization, the extent of ultrasonic transmission was displayed in the form of a red-to-blue heat map, where low transmission, represented by a blue color, corresponds to increased gas production (Figure 5e,f). In the case of the bare Li pouch cells, many blue areas were apparent after only 15 cycles, indicating gas generation. In contrast, no sign of gas bubbles is seen for the **WCOF**@Li anode system through 15 cycles (Figure 5g,h). This finding is taken as evidence that the **WCOF**@Li anode provides a stabilized electrode/electrolyte interface when incorporated into Li metal pouch cells.

3. Conclusion

In summary, we present a novel strategy for stabilizing lithium metal anodes through the design and application of a wavy covalent organic framework (**WCOF**) incorporating calix[4]pyrroles (**C4Ps**) units. By leveraging the intrinsic anion-binding capability of **C4Ps**, the **WCOF** selectively captures PF_6^- anions while maintaining efficient Li^+ transport, thus improving the interfacial ion dynamics. The unique wavy architecture of the framework, formed via self-assembly of C4P-based monomers, contributes to both the structural integrity of the **WCOF** and its functional performance. When employed as a protective coating, the **WCOF** of this study enables stable and reversible lithium plating/stripping over 2500 h at 1 mA cm^{-2} and 2 mAh cm^{-2}. Moreover, the coated anodes demonstrate excellent compatibility with high-voltage cathodes (NCM811 with a high mass loading of 20 mg cm^{-2}), underscoring the practicality of this interfacial engineering approach. Beyond its immediate application in lithium metal batteries, this work illustrates the broader potential of supramolecular design in tuning interfacial chemistry. In particular, applications of anion recognition chemistry within a porous framework is expected to open up new pathways for enhancing the stability and safety of next-generation energy storage systems.

Supporting Information

Supporting Information is available from the Wiley Online Library or from the author.

Acknowledgements

J.T. and Y.L. contributed equally to this work. X.C. is grateful to the National Natural Science Foundation of China (Grant No.22271110), Shenzhen Science and Technology Program (Grant No. GJHZ20240218114701003), and Natural Science Foundation of Hubei Province, China (Grant No. 2022CFA031) for financial support. The work in Austin was supported by the Robert A. Welch Foundation (F-0018) and the U.S. National Science Foundation (CHE-230473). The authors also thank the Analytical and Testing Center of Huazhong University of Science & Technology for providing analytical support. The authors also thank Prof. Xiaoyan Wang and Prof. Yong Yan for the helpful discussion involving the analysis of the WCOF structure.

Conflict of Interest

The authors declare no conflict of interest.

Data Availability Statement

The data that support the findings of this study are available in the supplementary material of this article.

Keywords

anion recognition, Calix[4]pyrrole, covalent organic frameworks, lithium anode protection, lithium metal battery

Received: May 27, 2025
Revised: June 18, 2025
Published online: July 28, 2025

[1] a) J. W. Choi, D. Aurbach, *Nat. Rev. Mater.* **2016**, *1*, 16013; b) Y. Liu, Q. Liu, L. Xin, Y. Liu, F. Yang, E. A. Stach, J. Xie, *Nat. Energy* **2017**, *2*, 17083; c) M. D. Tikekar, S. Choudhury, Z. Tu, L. A. Archer, *Nat. Energy* **2016**, *1*, 16114.

[2] a) Z. Huang, J.-C. Lai, S.-L. Liao, Z. Yu, Y. Chen, W. Yu, H. Gong, X. Gao, Y. Yang, J. Qin, Y. Cui, Z. Bao, *Nat. Energy* **2023**, *8*, 577; b) R. Weber, M. Genovese, A. J. Louli, S. Hames, C. Martin, I. G. Hill, J. R. Dahn, *Nat. Energy* **2019**, *4*, 683; c) J. Zhang, H. Zhang, S. Weng, R. Li, D. Lu, T. Deng, S. Zhang, L. Lv, J. Qi, X. Xiao, L. Fan, S. Geng, F. Wang, L. Chen, M. Noked, X. Wang, X. Fan, *Nat. Commun.* **2023**, *14*, 2211.

[3] H. Chen, Y. Yang, D. T. Boyle, Y. K. Jeong, R. Xu, L. S. de Vasconcelos, Z. Huang, H. Wang, H. Wang, W. Huang, H. Li, J. Wang, H. Gu, R. Matsumoto, K. Motohashi, Y. Nakayama, K. Zhao, Y. Cui, *Nat. Energy* **2021**, *6*, 790.

[4] a) L. Qiao, U. Oteo, M. Martinez-Ibañez, A. Santiago, R. Cid, E. Sanchez-Diez, E. Lobato, L. Meabe, M. Armand, H. Zhang, *Nat. Mater.* **2022**, *21*, 455; b) W. Xue, Z. Shi, M. Huang, S. Feng, C. Wang, F. Wang, J. Lopez, B. Qiao, G. Xu, W. Zhang, Y. Dong, R. Gao, Y. Shao-Horn, J. A. Johnson, J. Li, *Energy Environ. Sci.* **2020**, *13*, 212; c) W. Xue, M. Huang, Y. Li, Y. G. Zhu, R. Gao, X. Xiao, W. Zhang, S. Li, G. Xu, Y. Yu, P. Li, J. Lopez, D. Yu, Y. Dong, W. Fan, Z. Shi, R. Xiong, C.-J. Sun, I. Hwang, W.-K. Lee, Y. Shao-Horn, J. A. Johnson, J. Li, *Nat. Energy* **2021**, *6*, 495.

[5] a) M. S. Kim, Z. Zhang, P. E. Rudnicki, Z. Yu, J. Wang, H. Wang, S. T. Oyakhire, Y. Chen, S. C. Kim, W. Zhang, D. T. Boyle, X. Kong, R. Xu, Z. Huang, W. Huang, S. F. Bent, L.-W. Wang, J. Qin, Z. Bao, Y. Cui, *Nat. Mater.* **2022**, *21*, 445; b) A. J. Louli, A. Eldesoky, R. Weber, M. Genovese, M. Coon, J. deGooyer, Z. Deng, R. T. White, J. Lee, T. Rodgers, R. Petibon, S. Hy, S. J. H. Cheng, J. R. Dahn, *Nat. Energy* **2020**, *5*, 693; c) Z. Yu, H. Wang, X. Kong, W. Huang, Y. Tsao, D. G. Mackanic, K. Wang, X. Wang, W. Huang, S. Choudhury, Y. Zheng, C. V. Amanchukwu, S. T. Hung, Y. Ma, E. G. Lomeli, J. Qin, Y. Cui, Z. Bao, *Nat. Energy* **2020**, *5*, 526.

[6] a) A. P. Côté, A. I. Benin, N. W. Ockwig, M. O'Keeffe, A. J. Matzger, O. M. Yaghi, *Science* **2005**, *310*, 1166; b) C. S. Diercks, O. M. Yaghi,

Science **2017**, *355*, 6328; c) N. Huang, P. Wang, D. Jiang, *Nat. Rev. Mater.* **2016**, *1*, 16068; d) S. Kandambeth, K. Dey, R. Banerjee, *J. Am. Chem. Soc.* **2018**, *141*, 1807; e) S. J. Lyle, R. W. Flaig, K. E. Cordova, O. M. Yaghi, *J. Chem. Educ.* **2018**, *95*, 1512; f) P. J. Waller, F. Gándara, O. M. Yaghi, *Acc. Chem. Res.* **2015**, *48*, 3053; g) H. Xu, S. Tao, D. Jiang, *Nat. Mater.* **2016**, *15*, 722.

[7] C. S. Diercks, S. Lin, N. Kornienko, E. A. Kapustin, E. M. Nichols, C. Zhu, Y. Zhao, C. J. Chang, O. M. Yaghi, *J. Am. Chem. Soc.* **2018**, *140*, 1116.

[8] a) C. J. Doonan, D. J. Tranchemontagne, T. G. Glover, J. R. Hunt, O. M. Yaghi, *Nat. Chem.* **2010**, *2*, 235; b) H. L. Nguyen, N. Hanikel, S. J. Lyle, C. Zhu, D. M. Proserpio, O. M. Yaghi, *J. Am. Chem. Soc.* **2020**, *142*, 2218.

[9] V. S. Vyas, M. Vishwakarma, I. Moudrakovski, F. Haase, G. Savasci, C. Ochsenfeld, J. P. Spatz, B. V. Lotsch, *Adv. Mater.* **2016**, *28*, 8749.

[10] a) Y. Zhang, J. Duan, D. Ma, P. Li, S. Li, H. Li, J. Zhou, X. Ma, X. Feng, B. Wang, *Angew. Chem. Int. Ed. Engl.* **2017**, *56*, 16313; b) X. Li, Y. Tian, L. Shen, Z. Qu, T. Ma, F. Sun, X. Liu, C. Zhang, J. Shen, X. Li, L. Gao, S. Xiao, T. Liu, Y. Liu, Y. Lu, *Adv. Funct. Mater.* **2021**, *31*, 2009718; c) Y. Yuan, K. T. Bang, R. Wang, Y. Kim, *Adv. Mater.* **2023**, *35*, 2210952; d) C. Li, D.-D. Wang, G. S. H. Poon Ho, Z. Zhang, J. Huang, K.-T. Bang, C. Y. Lau, S.-Y. Leu, Y. Wang, Y. Kim, *J. Am. Chem. Soc.* **2023**, *145*, 24603; e) B. L. D. Rinkel, J. P. Vivek, N. Garcia-Araez, C. P. Grey, *Energy Environ. Sci.* **2022**, *15*, 3416.

[11] a) C. R. DeBlase, K. E. Silberstein, T.-T. Truong, H. D. Abruña, W. R. Dichtel, *J. Am. Chem. Soc.* **2013**, *135*, 16821; b) A. M. Evans, L. R. Parent, N. C. Flanders, R. P. Bisbey, E. Vitaku, M. S. Kirschner, R. D. Schaller, L. X. Chen, N. C. Gianneschi, W. R. Dichtel, *Science* **2018**, *361*, 52; c) Y. Liu, C. S. Diercks, Y. Ma, H. Lyu, C. Zhu, S. A. Alshmimri, S. Alshihri, O. M. Yaghi, *J. Am. Chem. Soc.* **2018**, *141*, 677; d) S. J. Lyle, P. J. Waller, O. M. Yaghi, *Trends Chem.* **2019**, *1*, 172; e) H. L. Nguyen, C. Gropp, Y. Ma, C. Zhu, O. M. Yaghi, *J. Am. Chem. Soc.* **2020**, *142*, 20335.

[12] a) B. Garai, D. Shetty, T. Skorjanc, F. Gándara, N. Naleem, S. Varghese, S. K. Sharma, M. Baias, R. Jagannathan, M. A. Olson, S. Kirmizialtin, A. Trabolsi, *J. Am. Chem. Soc.* **2021**, *143*, 3407; b) S. Huang, J. Y. Choi, Q. Xu, Y. Jin, J. Park, W. Zhang, *Angew. Chem., Int. Ed.* **2023**, *62*, 202303538.

[13] a) L. Escobar, Q. Sun, P. Ballester, *Acc. Chem. Res.* **2023**, *56*, 500; b) L. P. Skala, X. Aguilar-Enriquez, C. L. Stern, W. R. Dichtel, *Chem* **2023**, *9*, 709; c) J. L. Sessler, D. E. Gross, W.-S. Cho, V. M. Lynch, F. P. Schmidtchen, G. W. Bates, M. E. Light, P. A. Gale, *J. Am. Chem. Soc.* **2006**, *128*, 12281.

[14] J. H. Oh, B. P. Hay, V. M. Lynch, H. Li, J. L. Sessler, S. K. Kim, *J. Am. Chem. Soc.* **2022**, *144*, 16996.

[15] T. Hirao, D. S. Kim, X. Chi, V. M. Lynch, K. Ohara, J. S. Park, K. Yamaguchi, J. L. Sessler, *Nat. Commun.* **2018**, *9*, 823.

[16] M. Ciardi, A. Galán, P. Ballester, *J. Am. Chem. Soc.* **2015**, *137*, 2047.

[17] H. J. Clarke, E. N. W. Howe, X. Wu, F. Sommer, M. Yano, M. E. Light, S. Kubik, P. A. Gale, *J. Am. Chem. Soc.* **2016**, *138*, 16515.

[18] J. Aguilera-Sigalat, C. Sáenz de Pipaón, D. Hernández-Alonso, E. C. Escudero-Adán, J. R. Galan-Mascarós, P. Ballester, *Cryst. Growth Des.* **2017**, *17*, 1328.

[19] A. F. Sierra, D. Hernández-Alonso, M. A. Romero, J. A. González-Delgado, U. Pischel, P. Ballester, *J. Am. Chem. Soc.* **2020**, *142*, 4276.

[20] D. Luo, J. Tian, J. L. Sessler, X. Chi, *J. Am. Chem. Soc.* **2021**, *143*, 18849.

[21] a) S. Tan, Y. Jiang, S. Ni, H. Wang, F. Xiong, L. Cui, X. Pan, C. Tang, Y. Rong, Q. An, L. Mai, *Natl. Sci. Rev.* **2022**, *92*, 095; b) Y. Zhao, T. Zhou, T. Ashirov, M. E. Kazzi, C. Cancellieri, L. P. H. Jeurgens, J. W. Choi, A. Coskun, *Nat. Commun.* **2022**, *13*, 2575; c) Y. Zhang, Y. Wu, H. Li, J. Chen, D. Lei, C. Wang, *Nat. Commun.* **2022**, *13*, 1297; d) Y. Chen, Z. Yu, P. Rudnicki, H. Gong, Z. Huang, S. C. Kim, J.-C. Lai, X. Kong, J. Qin, Y. Cui, Z. Bao, *J. Am. Chem. Soc.* **2021**, *143*, 18703; e) Y. Huang, R. Li, S. Weng, H. Zhang, C. Zhu, D. Lu, C. Sun, X. Huang, T. Deng, L. Fan, L. Chen, X. Wang, X. Fan, *Energy Environ. Sci.* **2022**, *15*, 4349; f) M. Wu, Z. Wang, W. Zhang, C. Jayawardana, Y. Li, F. Chen, B. Nan, B. L. Lucht, C. Wang, *Angew. Chem., Int. Ed.* **2023**, *62*, 202216169; g) M. Zhu, Z. Fan, K. Xu, Y. Fang, W. Sun, Y. Zhu, *Adv. Funct. Mater.* **2022**, *32*, 2112645. h) Y. Li, Q. Guo, Y. Wu, D. Ying, Y. Yu, T. Chi, S. Xia, X. Zhou, Z. Liu, *Adv. Funct. Mater.* **2023**, *33*, 2214523; i) C. Liao, L. Han, W. Wang, W. Li, X. Mu, Y. Kan, J. Zhu, Z. Gui, X. He, L. Song, Y. Hu, *Adv. Funct. Mater.* **2023**, *33*, 2212605; j) Q. Liu, Y. Liu, Z. Chen, Q. Ma, Y. Hong, J. Wang, Y. Xu, W. Zhao, Z. Hu, X. Hong, J. Wang, X. Fan, H. B. Wu, *Adv. Funct. Mater.* **2022**, *33*, 1706102.

[22] Z. Deng, Z. Huang, Y. Shen, Y. Huang, H. Ding, A. Luscombe, M. Johnson, J. E. Harlow, R. Gauthier, J. R. Dahn, *Joule* **2020**, *4*, 2017.